Extreme Mechanics Letters 8 (2016) 13–21

Contents lists available at ScienceDirect

Extreme Mechanics Letters

journal homepage: www.elsevier.com/locate/eml

Mechanical interactions regulated kinetics and morphology of composite electrodes in Li-ion batteries

Rong Xu, Kejie Zhao *

School of Mechanical Engineering, Purdue University, West Lafayette, IN 47906, USA

ARTICLE INFO

Article history:
Received 15 September 2015
Received in revised form 8 October 2015
Accepted 29 October 2015
Available online 1 November 2015

Keywords:
Diffusion
Stress
Nanowire
Mechanical interactions
Li-ion batteries

ABSTRACT

Li-ion batteries are a system that features strong coupling between mechanical stresses and electrochemical reactions. Prior studies on stresses in electrodes are focused on single particles or mono-phase materials. The kinetics and morphology of composite electrodes regulated by the mechanical interactions are much less exploited. We integrate a continuum theory of coupled diffusion and large elasto-plastic deformation into a finite element program. Such a computational tool enables us to explore the intimate coupling between the lithiation kinetics and stresses in three-dimensional electrodes that are composed of multiple components. We find that Li profiles and stress states in multiple particles constrained by a matrix are significantly different from that in a free-standing configuration. The mechanical interactions regulate Li chemical potential in Si nanowires and transform the anisotropic deformation to an isotropic behavior and vice versa. The modeling is in good agreement with a recent experimental report.

© 2015 Elsevier Ltd. All rights reserved.

1. Introduction

Li-ion batteries are a key technology for portable electronics and electric vehicles [1–3]. The demand of lightweight, high-energy-density batteries has stimulated tremendous efforts from virtually all engineering disciplines [4]. Mechanical degradation has become a limiting factor for the commercialization of high-capacity electrodes. Such effects are exemplified in high-capacity anodes and Li-rich cathodes—large volumetric swelling and shrinking ranging from tens of percent to a few hundred percent occurs repetitively during the charge and discharge cycles [5–7]. Averting the mechanical degradation remains one of the major challenges for the development of high-performance batteries. On the frontier of mechanics, the kinetics of diffusive and interfacial reactions in the electrodes induces a wealth of intriguing phenomena, including cavitation [8–10], reactive plasticity [11,12] and corrosive fracture [13]. The electrochemical processes of Li insertion and extractions modulate large deformation and stress generation in the electrodes. Meanwhile, mechanical stresses significantly influence the thermodynamics and kinetics of lithiation reactions, ion diffusion, and phase transitions [14–18].

Numerical modeling is a common exercise to study the evolution of Li diffusion and the stress field in Li-ion batteries. However, prior research has been extensively focused on single particles or two-dimensional structures [19–25]. Bower and Guduru developed a finite element method to model diffusion, large deformation, and fracture [26], and the method was applied for a thin-film Si electrode [27]. Brassart et al. developed a finite element program to model the cyclic behavior of single spherical particles [28]; similar approach was adopted by Cui et al. [29]. An and Jiang reported a finite element package integrated in ABAQUS, and studied the failure mechanism in Si thin film bonded to a metal current collector [30]. Stein and Xu used isogeometric analysis to model the mechanical behaviors of single particles with different shapes [31]. Yang et al. recently developed a finite element program by manipulating the

* Corresponding author.
E-mail address: kjzhao@purdue.edu (K. Zhao).

http://dx.doi.org/10.1016/j.eml.2015.10.004
2352-4316/© 2015 Elsevier Ltd. All rights reserved.

stress effect on Li diffusivity, and studied the lithiation behavior of Si nanowires [32,33]. There are a few attempts in recent studies that incorporate a secondary component in the material model. Higa et al. simulated stresses in a two-dimensional cylindrical model that consists of a well-bonded binder with a cylindrical particle [34]. Rahani et al. studied the role of plastic deformation of binders on the stress evolution in the distributed spherical particles in a porous electrode by using a two-dimensional microstructural resolved model [35]. Nevertheless, the mechanical interactions among the different components and the stress effect on Li transport have not been considered. There has been a lack of computation tools to investigate the fully coupled diffusion and stress in three-dimensional composite configurations. Herein, we develop a finite element program based on a continuum theory of coupled diffusion and large elasto-plastic deformation. It enables us to model the complex behaviors of three-dimensional objects that are composed of multiple components and to explore the kinetics and morphological evolution of composite electrodes coupled with the mechanical interactions.

As pointed out by a recent experimental study on Si nanowires, lithiation often occurs simultaneously in a cluster of active materials in a mechanically confined medium [36]. The mechanical interactions among the individual Si structures in the closed space alter the reaction mechanisms along the various crystallographic orientations and enhance the fracture resistance of lithiated Si by mediating the stress concentrations. Indeed, distinct from the simplified single-particle or free-standing models, a battery electrode usually consists of multiple components with a large variation of mechanical properties [37]. The different components interact with each other during lithiation reactions and raise a complex field of stresses. We demonstrate that single-particle models are unable to capture the mechanical behaviors of a composite electrode due to the strong coupling between Li transport and stresses. In a model of multiple particles embedded in a matrix, we find that Li profiles and the stress field are highly asymmetric due to the matrix confinement and particle interactions. In another example of multiple Si nanowires in a confined space, the mechanical stress regulates the Li chemical potential, redistributes the Li concentration, and transforms the anisotropic deformation of nanowires to an isotropic behavior and vice versa. Such findings are in good agreement with the experimental report [36].

2. Theory and finite element modeling

As the first attempt to model the composite electrodes, we consider three-dimensional material models consisting of two components—active and inactive materials, where Li diffusion only occurs in the active material while the inactive material provides mechanical confinement. This is an assumption based on the fact that the kinetics in batteries is often limited by the diffusion in the active materials while Li transport through the porous matrix is usually a faster process. In the reference state, both components are free of Li and stresses. Lithiation is induced by imposing a nominal influx J_0 of Li on the surface of the active material. The concurrent diffusion and large elasto-plastic deformation is described by a previous developed theory by Zhao et al. [38]. In brevity, the mechanical equilibrium is represented as follows,

$$\nabla \cdot \mathbf{S} + \mathbf{F_b} = 0 \tag{1}$$

where $\mathbf{S}$ is the nominal stress calculated as $\mathbf{S} = \mathbf{K} : \boldsymbol{\varepsilon}_\mathbf{e}$, $\mathbf{K}$ the stiffness matrix, $\boldsymbol{\varepsilon}_\mathbf{e}$ the elastic strain, $\mathbf{F_b}$ the body force. The total deformation of a representative material element is treated to follow the kinematic multiplicative decomposition $F = F_e F_l F_p$, where F represents the deformation gradient, F_e the reversible elastic distortion of the material, F_l lithiation-induced volumetric deformation, and F_p the irreversible plastic deformation that dictates the shape change of the body. The elastic strain is computed as $\boldsymbol{\varepsilon}_\mathbf{e} = \frac{1}{2}(\mathbf{F}_\mathbf{e}^\mathbf{T}\mathbf{F}_\mathbf{e} - \mathbf{I})$. The volumetric change due to Li insertion is $1 + \Omega C$, where Ω and C are the partial molar volume and concentration of Li, respectively. The material element yields under the von Mises conditions and the plastic deformation follows the J_2 flow theory. For the inactive material, the deformation and stresses are caused by the mechanical interactions with the active material. Its constitutive behavior is described by a Neo-Hookean material model [39].

The kinetics of Li diffusion is described as follows. Let C be the nominal concentration of Li (i.e., the number of Li atoms per unit volume of active materials in the reference state). Let $\boldsymbol{J}$ be the nominal flux of Li (i.e., the number of Li atoms per unit reference area per unit time). Conservation of the number of Li atoms requires that

$$\frac{\partial C}{\partial t} + \nabla \cdot \boldsymbol{J} = 0, \tag{2}$$

where ∇ represents the gradient with respect to the material (or Lagrangian) coordinate. Let $\boldsymbol{j}$ be the true flux of Li (i.e., the number of Li atoms per unit area per unit time in the spatial (or Eulerian) coordinate). It is taken to depend on the spatial gradient of the chemical potential μ, $\boldsymbol{j} = -\frac{cD}{kT}\nabla_{x_i}\mu$, where D is a constant diffusion coefficient, kT the temperature in the unit of energy, c the true concentration of Li in the spatial coordinate, and the ∇_{x_i} gradient with respect to the spatial coordinate. Using the standard transformation rules of continuum mechanics, the relationship between the nominal flux and the chemical potential in the Lagrangian coordinate can be obtained as $\boldsymbol{J} = -\frac{CD}{kT}F^{-1}F^{-T}\nabla\mu$. The boundary conditions are prescribed as follows. We prescribe a zero displacement condition at the center of the active materials during Li insertion to prevent the rigid motion, $\mathbf{u}(0, t) = 0$. For the diffusion boundary condition, we assume good ionic and electronic conductivities of the inactive materials such that each active material experiences the same current. We impose a nominal flux $\boldsymbol{J}$ on the surface of the particles with a constant value J_0.

The governing equations for the kinematics of deformation and the kinetics of diffusion are both strongly nonlinear. We integrate their weak formulations into the finite element program within a Lagrangian setting. The coupled equations for stress equilibrium and Li diffusion are solved simultaneously at every time step. The weak form for the

mechanical equilibrium equation is obtained by multiplying Eq. (1) by a test function and integrating it over the volume of the material.

$$\int_{\Omega} (\nabla \cdot \mathbf{S} + \mathbf{F_b}) \cdot \mathbf{v} dV = 0, \tag{3}$$

where $\mathbf{v}(X_i, t)$ is a test function that vanishes on the boundary. Integrating Eq. (3) by parts, we obtain that

$$\int_{\Omega} \mathbf{S} \cdot \nabla \mathbf{v} d\Omega - \int_{\Omega} \mathbf{F_b} \cdot \mathbf{v} d\Omega - \int_{\partial\Omega} \mathbf{P} \cdot \mathbf{v} dS = 0, \tag{4}$$

where $\mathbf{P}$ represents the surface traction. Following the similar procedure, the weak form for the mass transport is obtained as follows,

$$\int_{\Omega} \left(\frac{\partial C}{\partial t} \hat{\mu} - \boldsymbol{J} \cdot \nabla \hat{\mu} \right) dV + \int_{\partial\Omega} (\boldsymbol{N} \cdot \boldsymbol{J}) \hat{\mu} dS = 0, \tag{5}$$

where $\boldsymbol{N} \cdot \boldsymbol{J} = J_0$, and $\hat{\mu}(X_i, t)$ is a test function. The weak form Eq. (5) suggests that the chemical potential $\mu(X_i, t)$ is used as the field variable for Li transport, instead of the use of concentration $C(X_i, t)$. The true Li concentration c can be computed from the chemical potential and the mean stress σ_m by $c = \exp\{(\mu - \mu_0 + \Omega\sigma_m)/kT\}/\Omega$ and the nominal concentration is calculated by $C = c \cdot \det(\mathbf{F})$. Such a choice is beneficial for the numerical convergence. To solve the coupled problem, we implement the weak formulations into the commercial software COMSOL Multiphysics. We use the built-in time-dependent solver MUMPS (MUltifrontal Massively Parallel sparse direct Solver) to solve the co-evolution of Li concentration and stresses [40]. To improve the convergence, the segregated approach is adopted.

3. Li diffusion and stresses in particle/matrix composite electrodes

We simulate three sets of material models to assess the effect of mechanical interactions on the co-evolution of Li diffusion and the stress field—a single free-standing particle, a particle embedded in a matrix, and multiple particles confined in a matrix. Amorphous Si is taken as the model system for the active material and typical polymer binders are taken as an example of inactive matrix. The radius of Si spherical particles is set to be $A = 1$ μm. The size of the matrix and the spacing between the particles are varied to tune the mechanical interactions. The material parameters are adopted as follows. For Si particles, Young's modulus $E_P = 80$ GPa, Poisson's ratio $\nu_P = 0.3$, yield strength $\sigma_Y = 0.5$ GPa, Li diffusivity $D = 10^{-16}$ m^2/s, partial molar volume of Li in Si $\Omega = 1.36 \times 10^{-29}$ m^3, the activity coefficient $\gamma = 1$, and temperature $T = 300$ K [41,42]. It is worth noting that Young's modulus, yield strength, and Li diffusivity of lithiated Si may depend on the Li composition. Here we keep the material parameters as constants to reduce the complexity of the modeling. For the matrix, Poisson's ratio $\nu_M = 0.3$, and Young's modulus E_M are varied in the range of 260 MPa to 2.6 GPa. The volumetric strain of Si upon full lithiation is about 300% which sets the relationship $\Omega C_{\max} = 3$, where $C_{\max}$ represents the maximum Li concentration. The charging time to reach the theoretical capacity of Si is set to be $\tau = 1$ h. The nominal flux J_0 is then determined through the relationship $4A^2 J_0 = (4A^3/3) C_{\max}$. At the charging rate $\tau = 1$ h, $J_0 = 2.8D/A$. Li insertion is terminated when the concentration on the particle surface reaches $C_{\max}$.

Single free-standing particles have been examined in several past studies which often treat a spherical particle as a one-dimensional model by taking into account the symmetry. Here we start with a full three-dimensional spherical model to verify the finite element program and to demonstrate the different features of single particles versus composite configurations. Fig. 1(a) and (b) show the distribution of Li concentration and the corresponding equivalent stress along the radius of the Si particle at the normalized charging time $\bar{t} = Dt/A^2$. The chemical potential of Li in the particle drives Li diffusion from the surface toward the center. At a fast charging rate relative to the diffusion rate of Li, the particle expands more near the surface than at the center, resulting in a compressive stress field near the surface and a tensile stress field at the center. For the spherical particle, the equivalent stress is $\sigma_e = |\sigma_\theta - \sigma_r|$, which is bounded in the interval $0 \le \sigma_e \le \sigma_Y$. Fig. 1(b) shows the evolution of the equivalent stress. The gradient of the mean stress promotes Li diffusion toward the center and tends to homogenize the Li distribution. Such a homogenization effect consequently reduces the stresses and induces elastic unloading in the plastic regime. As evident in Fig. 1(b), the spherical particle experiences plastic yielding and elastic unloading in the course of Li insertion. We compare the results with a previous study by Brassart et al. which used one-dimensional finite element formulation [28]. The Li profiles and stress states at each time step are in excellent agreement.

For comparison, we study the lithiation behavior of an elliptical Si particle to demonstrate the geometric effect. We set the two semi-minor radii of the ellipse as A and the semi-major radius being $A_e = 1.5A$. The charging time to reach the theoretical capacity remains $\tau = 1$ h. Fig. 1(c) shows the distribution of Li concentration along the semi-major axis. The Li profile is inhomogeneous within the elliptical particle as indicated by the inset figure of Fig. 1(c)—the area near the end of the semi-major axis is fully lithiated in a short time while other regimes remain at fairly low Li concentrations. Such inhomogeneity is dominated by the geometric effect that the uniform influx J_0 leads to a larger Li concentration near the semi-major axis which has a smaller effective radius. The geometric asymmetry also results in different elasto-plastic behaviors. The center of the elliptical particle is subjected to non-hydrostatic stresses. Fig. 1(d) plots the evolution of the equivalent stress. The equivalent stress at the center steadily increases until it reaches the yield strength. The outer shell experiences plastic yielding and then elastic unloading due to the homogenization effect of the stress gradient to the Li distribution.

The diffusion kinetics in composite electrodes coupled with the mechanical interactions has not been explored in prior studies. We consider the simple cases that a spherical particle embedded in a matrix to demonstrate the distinct behaviors of composite structures versus the single particles. It is noted that the material models considered

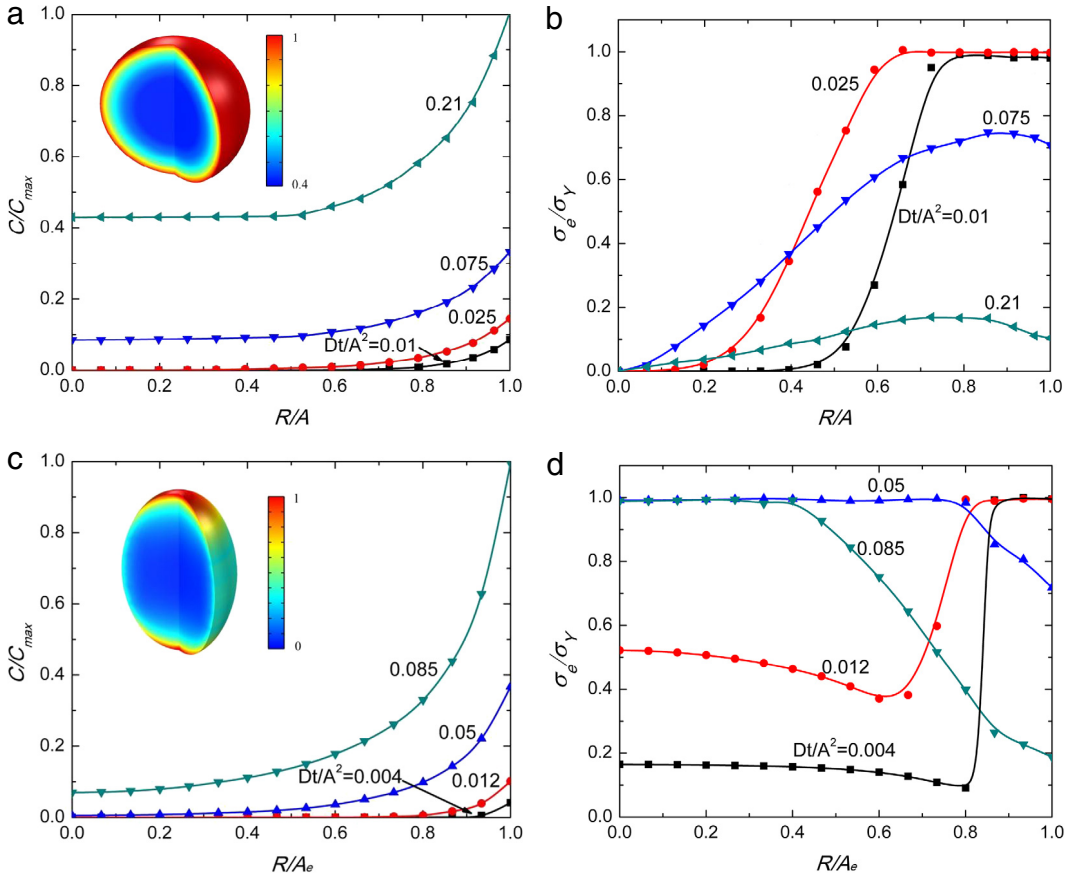

Fig. 1. (a) Distribution of Li concentration along the radius of a three-dimensional spherical Si particle under the lithiation rate $\tau = 1$ h. (b) The corresponding evolution of the equivalent stress. The particle experiences plastic yielding and elastic unloading in the course of Li insertion. (c) Distribution of Li concentration along the semi-major axis of a three-dimensional elliptical Si particle. (d) The corresponding evolution of the equivalent stress. The elasto-plastic behavior is distinct from that of spherical particles due to the geometric asymmetry.

here are yet to be close to the real configurations in commercial batteries, however, we may take the examples to uncover the elementary coupling between the lithiation kinetics and mechanical stresses in three-dimensional structures. Fig. 2(a) sketches the different elasto-plastic behaviors of a spherical particle embedded in a matrix of different stiffness and of different boundary conditions. For a single free-standing Si particle, Fig. 1(b) shows that the outer shell experiences a transition of plastic yielding to elastic unloading while the center remains elastic. Such a behavior is expected for a spherical particle embedded in a sufficiently compliant matrix of free boundary conditions. When the stiffness of the matrix increases, the matrix imposes a strong mechanical constraint to the deformation of the particle. The constraint imposes a hydrostatic stress to the center of the particle. However, for the outer shell, the compressive stress induced by the matrix may override the stress relaxation caused by the homogenization of Li distribution and lead to a permanent plastic deformation. The stress evolution will be altered by prescribing a periodic boundary condition (P. B. C) along the horizontal direction as if we consider the interactions between the particles. The simultaneous swelling of the neighboring particles in the confined space results in a non-hydrostatic stress field that effectively promotes the plastic yielding of the particles. As a result, the entire particle will reach plasticity progressively from the surface toward the center during the Li insertion. Fig. 2(b) shows an example of the equivalent stresses for $E_M/E_P = 0.032$ and $2A/L = 0.67$. The mechanical interactions are dependent on the stiffness ratio E_M/E_P and the size ratio $2A/L$ between the matrix and the particle. For a particle–matrix composite of small values of E_M/E_P and $2A/L$, the elasto-plastic behavior reduces to that of a single free-standing particle.

For the composite electrodes in batteries, mechanical failure often occurs by the structural disintegration due to the fracture of the conductive matrix or interfacial debonding between the active material and the matrix. Such failure mechanisms may be dictated by the tensile and shear stresses in the matrix. Fig. 2(c) shows the profiles of the maximum tensile and shear stresses in the matrix as a function of $2A/L$ at the time that the particle is fully lithiated. We find that the maximum stresses in the matrix are always located near the particle/matrix interface during lithiation. The tensile stress may cause fracture of the matrix initiated from the interface, and the shear stress may cause the interfacial debonding between the particles and the matrix. Fig. 2(c) shows that, for

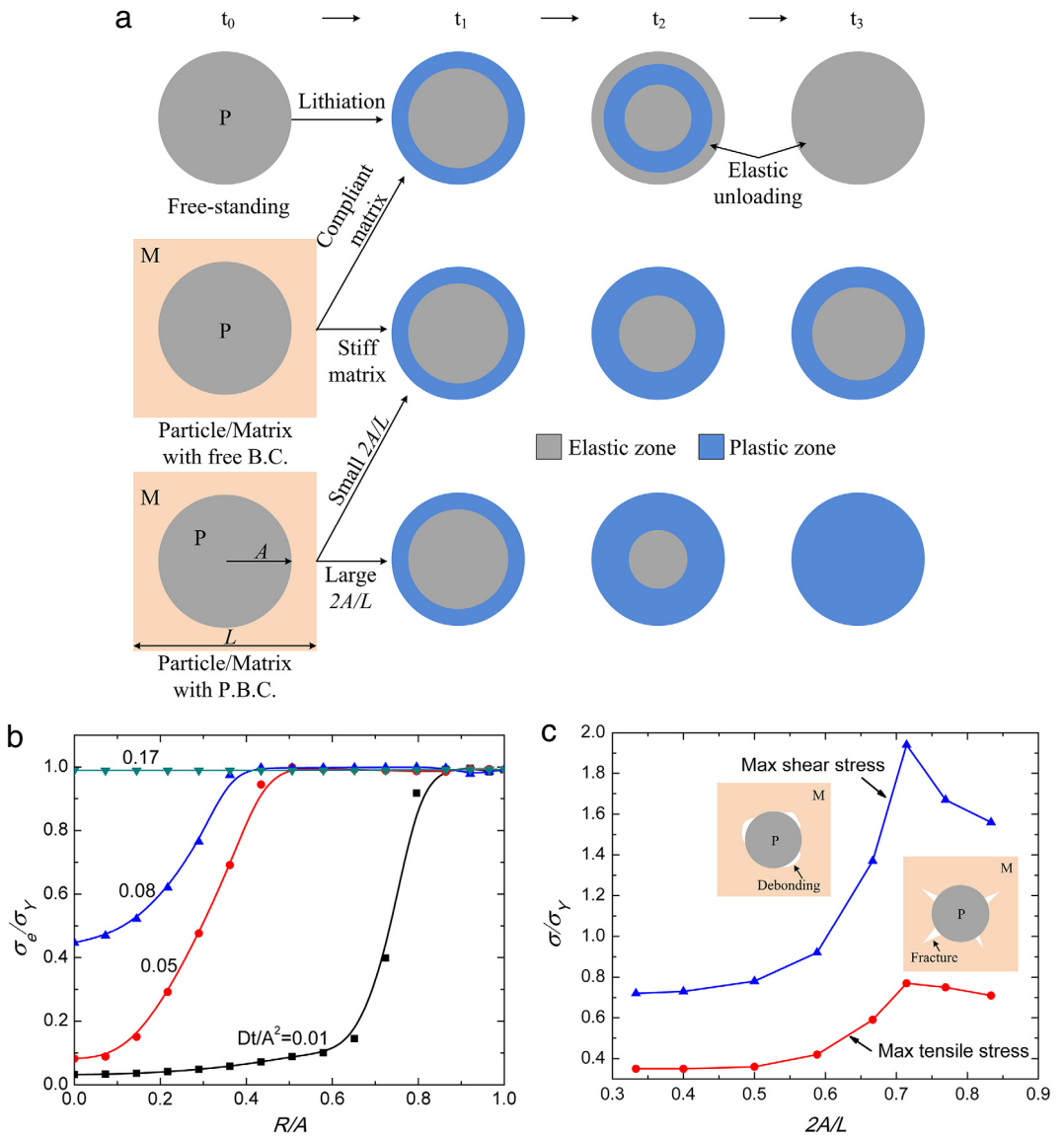

Fig. 2. (a) Schematic of the stress evolution in a single free-standing particle vs. a particle embedded in a matrix of different stiffness and under different boundary conditions. The particle is subjected to a constant charging rate. (b) Evolution of the equivalent stress in a particle embedded in a matrix of stiffness $E_M/E_P = 0.032$. The size ratio is $2A/L = 0.67$. Periodic boundary condition is applied along the horizontal direction. The charging rate is $\tau = 1$ h. (c) The profile of the maximum tensile and shear stresses in the matrix as a function of 2A/L. The particle is at the fully charged state. The tensile stress may cause fracture of the matrix, and the shear stress may cause interfacial debonding between the particle and the matrix.

$2A/L = 0.71$, the maximum tensile and shear stresses in the matrix reach peak values, which are on the same magnitude of the yield strength of the active particle. Such large stresses are hardly sustainable for the polymer matrix.

In the next example, we consider multiple particles embedded in a matrix to demonstrate the inhomogeneity of Li distribution regulated by the mechanical stresses. Fig. 3(a) shows three particles of a relatively large spacing in between. Li concentration shows a homogeneous distribution as there are minor mechanical interactions between the particles. As the particle distance decreases, Fig. 3(b), a highly asymmetric stress field develops in the particles which consequently redistributes the Li concentrations. The largest compressive stress occurs at the point in a particle of the shortest distance to the neighboring particles, so does the Li chemical potential. The variation of the Li chemical potential depends on the magnitude of the local compressive stress. Li atoms are then accumulated in the region of the lowest Li chemical potential. We use $C_{\min}/C_{\max}$ to dictate the inhomogeneity of Li distribution, where $C_{\min}$ represents the minimum Li concentration on the surface of the particle at the fully lithiated state. The inhomogeneity quantity depends on a set of dimensionless parameters $\left(A/L, E_M/E_P, L^2/D\tau, t/\tau\right)$, where A/L, E_M/E_P, $L^2/D\tau$, and t/τ represent the normalized particle spacing, matrix stiffness, charging rate, and charging time, respectively. Through parametric studies, we obtain

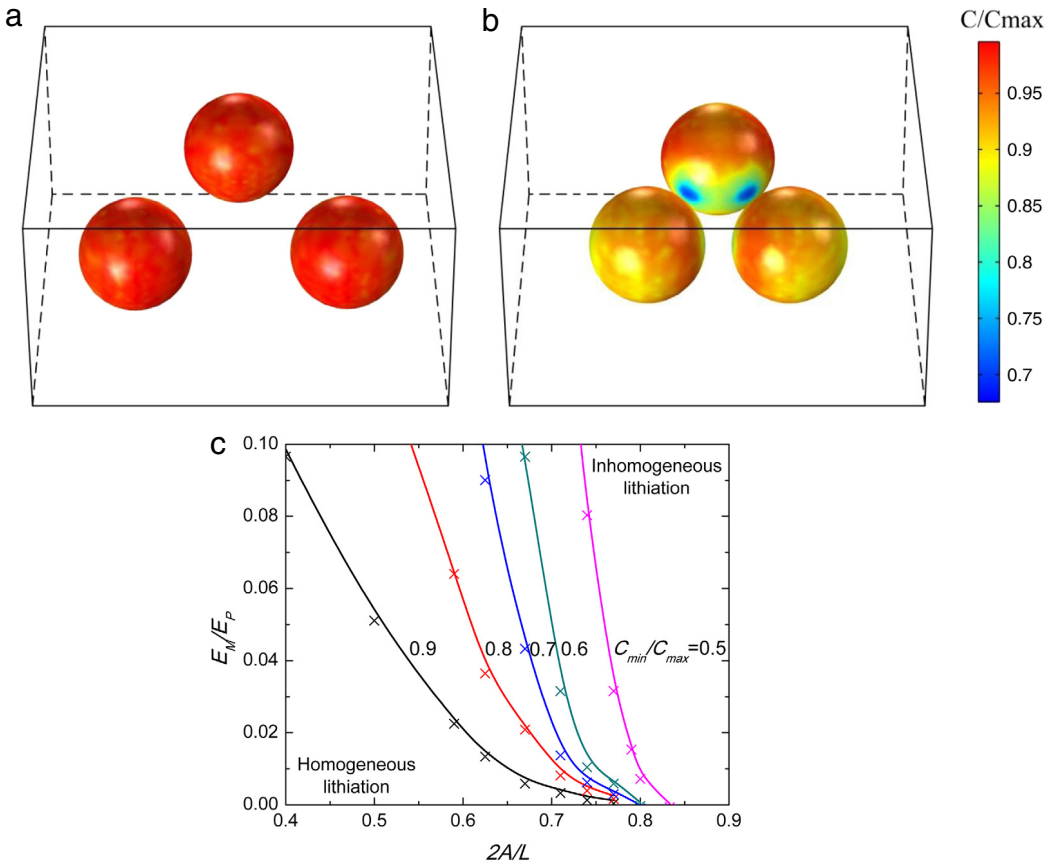

Fig. 3. (a) The homogeneous distribution of Li concentration in three particles with a relatively large space in between. (b) The highly inhomogeneous distribution of Li concentration due to the mechanical interactions of the three particles when they are close to each other. (c) The inhomogeneity of Li concentration distribution in terms of the non-dimensional quantities E_M/E_P and $2A/L$.

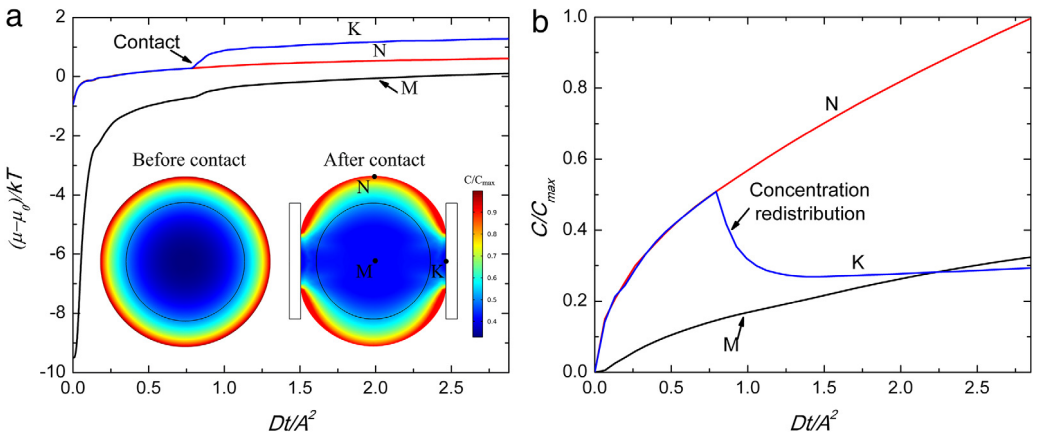

Fig. 4. The morphological evolution of a single amorphous Si nanowire regulated by the contact force. The compressive force between the nanowire and the rigid wall modulates the Li chemical potential and distribution of Li concentration, and thus transfer the isotropic deformation to an anisotropic behavior. (a) The distribution of Li chemical potential at different locations, marked by M, N, and K, before and after the Si nanowire contacts the rigid wall. (b) The evolution of Li profiles at the different locations. The contact force at K redistributes the Li concentration and leads to the anisotropic deformation.

the inhomogeneity in terms of E_M/E_P and A/L, as shown in Fig. 3(c). As expected, for the small values of E_M/E_P and A/L, the particles approach to a homogeneous lithiation. In the other limit of large E_M/E_P and A/L, the effect of the mechanical interactions on the Li distribution becomes dominant and the Li profiles are highly inhomogeneous. In this case, insertion of Li is blocked by the local high compressive stress that significantly reduces the effective capacity of the Si particles. It shows the fact that the capacity of the composite electrodes is not linearly scaled with the mass

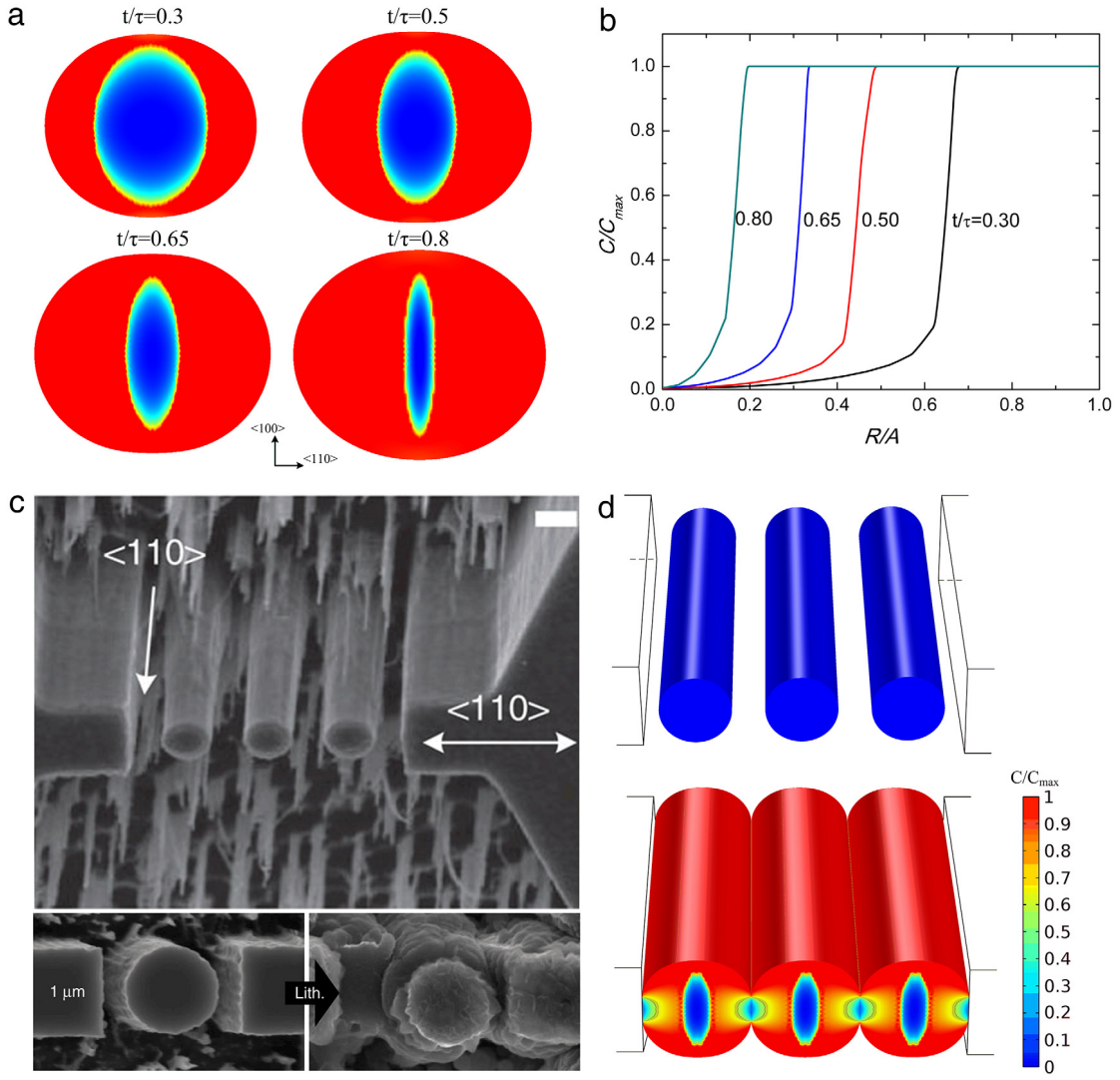

Fig. 5. The morphological evolution of a single crystalline Si nanowire vs. multiple nanowires. (a) The anisotropic deformation of a single crystalline nanowire induced by the concurrent interfacial reaction and plasticity. The propagation of the sharp lithiation front is simulated by setting $V_{110}/V_{100} = 5$ and $D_L/D_C = 10^4$. (b) The corresponding Li profiles at different charging time. (c) An experimental study of multiple nanowires shows that the mechanical interactions regulate the kinetics of lithiation and morphological evolution of the nanowires. Reproduced with permission from Lee et al. *Nature Communications*, 7533, 2015, by the Nature Publishing Group. (d) Finite element simulations on the experimental setting capture the transition from the anisotropic deformation to an isotropic behavior due to the stress effect.

of the active materials but is rather limited by the inhomogeneous storage of Li. An optimum structure of composite electrodes of mechanical resilience and effective Li storage can be designed by tuning the parameters of the stiffness of the matrix, the size, shape, and pattern of active particles, as well as the geometry and porosity of the matrix.

4. Lithiation of Si nanowires

The mechanical degradation of high-capacity electrodes motivated researchers to seek solutions from the nanotechnology, which has enabled low-cost, fast fabrications of nanostructured materials with nanoscale controls on the size, shape, and chemical compositions. As the characteristic size of the electrode materials scales down to the nanometer range, it can mitigate mechanical degradation through manipulating the deformation pattern. Furthermore, the small feature size enables flaw tolerance, facilitates ion and electron conduction, and promotes the rate capability by increasing the surface area of the electrodes to react with Li. Nanoelectrodes of different geometrical shapes have been assessed in a variety of electrodes, including nanowires [43], nanotubes [44], thin films [45], and nanoparticles [46]. We employ the finite element program to model the lithiation behavior of nanowires which have shown a great promise for the commercialization of Si electrodes. We study two example systems—a single amorphous Si nanowire as well as a cluster of crystalline Si nanowires both lithiated in a confined space. The goal is to demonstrate the mechanical stresses regulated lithiation kinetics and morphological evolution of the nanowires,

that is, the local contact force drives Li flux and dynamically changes the composition in the contact area and therefore modulates the deformation behavior. Understanding such a coupling effect is significant for the design of nanostructures to reach the optimum capacity and for the assessment of the mechanical performance of the electrodes.

We first model the lithiation-induced deformation in an amorphous Si nanowire confined by the side rigid walls, in which the radius of the nanowire is 275 nm. Fig. 4(a) and (b) show the distributions of Li chemical potential and Li concentrations at the different locations, marked by M, N, and K, as a function of the charging time. In Fig. 4(a), the jump in the Li chemical potential at K indicates the initial contact of the nanowire with the rigid wall. The confinement generates a large local compressive stress and drastically alters the profile of the Li chemical potential as shown in Fig. 4(a). The local contact force drives Li flux away from the stressed area. Li concentration at K gradually decreases until it reaches a steady state as shown in Fig. 4(b). This behavior infers that any contact forces, such as the mechanical load in the indentation experiments, may dynamically change the local composition at the measured regime. In order to accurately map the Li profile and the mechanical properties, one needs to consider the dynamic nature of Li diffusion, the stress-relaxation mechanisms in the electrodes, as well as the magnitude of the local forces. The morphological evolution is associated with the redistribution of Li concentrations. The contact force transfers the isotropic deformation of an amorphous nanowire to an anisotropic behavior, as shown in the inset figures of Fig. 4(a).

The lithiation mechanism of crystalline Si is different from that of amorphous Si. The reaction front separating the crystalline Si and lithiated amorphous phase is atomically sharp which is indicative of distinction from the diffusive behavior. The rate of lithiation in crystalline Si is limited by the short-range processes of interfacial reactions and the deformation is governed by the concurrent reaction and plasticity [47]. We simulate the sharp interface by adopting a step function of Li diffusivity $D_L/D_C = 10^4$, where D_L represents Li diffusivity in the lithiated phase, and D_C the diffusivity in the pristine core. Meanwhile we prescribe a constant velocity V to the step function along the radial direction of the Si nanowire to represent the propagation of the reaction front. Since the reaction rates along various crystallographic orientations are different, we set the reaction rates along the $\langle 110\rangle$ and $\langle 100\rangle$ direction as $V_{110}/V_{100} = 5$ [48]. It is worth noting that such a numerical approach is not aiming to incorporating a physical model on the short-range processes of bond switching, instead it serves as a means to model the kinetics of lithiation that is limited at the reaction front. The anisotropic deformation of a single crystalline nanowire and the movement of the sharp interface in the course of lithiation are shown in Fig. 5(a). The corresponding Li profiles at different charging time are plotted in Fig. 5(b). Next we simulate lithiation of a cluster of Si nanowires—three crystalline nanowires confined by rigid walls to compare with the recent experimental study. Fig. 5(c) reproduces the experimental figure that the mechanical interactions among the individual nanowires and the confined medium regulate the morphological evolution of the nanowires [36]. The numerical results shown in Fig. 5(d) are in excellent agreement with the experimental finding. The contact forces transfer the anisotropic deformation of crystalline nanowires to an isotropic behavior due to the redistribution of Li concentrations. Such transition mitigates the stress concentrations in single nanowires and thus results in a higher fracture resistance in the cluster of nanowires.

5. Conclusion

We develop a finite element program based on a theory of coupled diffusion and large elasto-plastic deformation. The program enables us to model the chemomechanical behaviors of three-dimensional composite electrodes and to explore the intimate coupling between the lithiation kinetics and mechanical stresses. We find that the Li profiles and stress states in multiple particles constrained by a matrix are significantly different from that in a free-standing configuration. We show that the capacity and stresses of the composite electrodes can be optimally designed by tuning the size, shape, and pattern of the active particles, as well as the stiffness, geometry, and porosity of the matrix. The mechanical interactions regulate Li chemical potential in Si nanowires and transform the isotropic deformation to an anisotropic behavior and vice versa. The modeling highlights the strong coupling between the electrochemistry of lithiation and mechanical stresses in the composite electrodes and provides important insight on the design of resilient Li-ion batteries.

Acknowledgments

The research project is supported by the start-up funds at Purdue University. We are grateful for the support of Haythornthwaite Foundation Initiation Grant from American Society of Mechanical Engineering.

References

[1] M. Armand, J.M. Tarascon, Building better batteries, Nature 451 (2008) 652.
[2] M.S. Whittingham, Materials challenges facing electrical energy storage, MRS Bull. 33 (2008) 411.
[3] B. Scrosati, J. Garche, Lithium batteries: status, prospects and future, J. Power Sources 195 (2010) 2419.
[4] N. Nitta, F. Wu, J.T. Lee, G. Yushin, Li-ion battery materials: present and future, Mater. Today 18 (2015) 252.
[5] L. Beaulieu, K. Eberman, R. Turner, L. Krause, et al., Colossal reversible volume changes in lithium alloys, Electrochem. Solid State Lett. 4 (2001) A137.
[6] Hyea Kim, Jung Tae Lee, Alexandre Magasinski, Kejie Zhao, et al., In-situ TEM observation of electrochemical lithiation of sulfur confined within inner cylindrical pores of carbon nanotubes, Adv. Energy Mater. (2015) 1501306. http://dx.doi.org/10.1002/aenm.201501306.
[7] J. Li, B.L. Armstrong, J. Kiggans, C. Daniel, et al., Lithium ion cell performance enhancement using aqueous $LiFePO_4$ cathode dispersions and polyethyleneimine dispersant, J. Electrochem. Soc. 160 (2013) A201.
[8] J.W. Choi, J. McDonough, S. Jeong, J.S. Yoo, et al., Stepwise nanopore evolution in one-dimensional nanostructures, Nano Lett. 10 (2010) 1409.
[9] X.H. Liu, S. Huang, S.T. Picraux, J. Li, et al., Reversible nanopore formation in Ge nanowires during lithiation–delithiation cycling: an in situ transmission electron microscopy study, Nano Lett. 11 (2011) 3991.
[10] K. Zhao, W.L. Wang, J. Gregoire, M. Pharr, et al., Lithium-assisted plastic deformation of silicon electrodes in lithium-ion batteries: a first-principles theoretical study, Nano Lett. 11 (2011) 2962.

[11] K. Zhao, G.A. Tritsaris, M. Pharr, W.L. Wang, et al., Reactive flow in silicon electrodes assisted by the insertion of lithium, Nano Lett. 12 (2012) 4397.
[12] L. Brassart, Z. Suo, Reactive flow in solids, J. Mech. Phys. Solids 61 (2013) 61.
[13] X. Huang, H. Yang, W. Liang, M. Raju, et al., Lithiation induced corrosive fracture in defective carbon nanotubes, Appl. Phys. Lett. 103 (2013) 153901.
[14] K. Zhao, M. Pharr, Q. Wan, W.L. Wang, et al., Concurrent reaction and plasticity during initial lithiation of crystalline silicon in lithium-ion batteries, J. Electrochem. Soc. 159 (2012) A238.
[15] M.T. McDowell, S.W. Lee, C. Wang, W.D. Nix, et al., Studying the kinetics of crystalline silicon nanoparticle lithiation with in situ transmission electron microscopy, Adv. Mater. 24 (2012) 6034.
[16] H. Yang, W. Liang, X. Guo, C.M. Wang, et al., Strong kinetics-stress coupling in lithiation of Si and Ge anodes, Extreme Mech. Lett. 2 (2015) 1.
[17] G. Sandu, L. Brassart, J.F. Gohy, T. Pardoen, et al., Surface coating mediated swelling and fracture of silicon nanowires during lithiation, ACS Nano 8 (2014) 9427.
[18] A. Mukhopadhyay, B.W. Sheldon, Deformation and stress in electrode materials for Li-ion batteries, Prog. Mater. Sci. 63 (2014) 58.
[19] M.W. Verbrugge, B.J. Koch, Modeling lithium intercalation of single-fiber carbon microelectrodes, J. Electrochem. Soc. 143 (1996) 600.
[20] J. Christensen, J. Newman, Stress generation and fracture in lithium insertion materials, J. Solid State Electrochem. 10 (2006) 293.
[21] X. Zhang, W. Shyy, A.M. Sastry, Numerical simulation of intercalation-induced stress in Li-ion battery electrode particles, J. Electrochem. Soc. 154 (2007) A910.
[22] Y.T. Cheng, M.W. Verbrugge, Evolution of stress within a spherical insertion electrode particle under potentiostatic and galvanostatic operation, J. Power Sources 190 (2009) 453.
[23] S. Golmon, K. Maute, S.H. Lee, M.L. Dunn, Stress generation in silicon particles during lithium insertion, Appl. Phys. Lett. 97 (2010) 033111.
[24] H. Haftbaradaran, X. Xiao, M.W. Verbrugge, H. Gao, Method to deduce the critical size for interfacial delamination of patterned electrode structures and application to lithiation of thin-film silicon islands, J. Power Sources 206 (2012) 357.
[25] Y. Gao, M. Zhou, Strong stress-enhanced diffusion in amorphous lithium alloy nanowire electrodes, J. Appl. Phys. 109 (2011) 014310.
[26] A.F. Bower, P.R. Guduru, V.A. Sethuraman, A finite strain model of stress, diffusion, plastic flow, and electrochemical reactions in a lithium-ion half-cell, J. Mech. Phys. Solids 59 (2011) 804.
[27] A. Bower, P. Guduru, A simple finite element model of diffusion, finite deformation, plasticity and fracture in lithium ion insertion electrode materials, Model. Simul. Mater. Sci. Eng. 20 (2012) 045004.
[28] L. Brassart, K. Zhao, Z. Suo, Cyclic plasticity and shakedown in high-capacity electrodes of lithium-ion batteries, Int. J. Solids Struct. 50 (2013) 1120.
[29] Z. Cui, F. Gao, J. Qu, A finite deformation stress-dependent chemical potential and its applications to lithium ion batteries, J. Mech. Phys. Solids 60 (2012) 1280.
[30] Y. An, H. Jiang, A finite element simulation on transient large deformation and mass diffusion in electrodes for lithium ion batteries, Model. Simul. Mater. Sci. Eng. 21 (2013) 074007.
[31] P. Stein, B. Xu, 3D Isogeometric analysis of intercalation-induced stresses in Li-ion battery electrode particles, Comput. Methods Appl. Mech. Engrg. 268 (2014) 225.
[32] H. Yang, S. Huang, X. Huang, F. Fan, et al., Orientation-dependent interfacial mobility governs the anisotropic swelling in lithiated silicon nanowires, Nano Lett. 12 (2012) 1953.
[33] H. Yang, F. Fan, W. Liang, X. Guo, et al., A chemo-mechanical model of lithiation in silicon, J. Mech. Phys. Solids 70 (2014) 349.
[34] K. Higa, V. Srinivasan, Stress and strain in silicon electrode models, J. Electrochem. Soc. 162 (2015) A1111.
[35] E.K. Rahani, V.B. Shenoy, Role of plastic deformation of binder on stress evolution during charging and discharging in lithium-ion battery negative electrodes, J. Electrochem. Soc. 160 (2013) A1153.
[36] S.W. Lee, H.W. Lee, I. Ryu, W.D. Nix, et al., Kinetics and fracture resistance of lithiated silicon nanostructure pairs controlled by their mechanical interaction, Nature Commun. 6 (2015) 7533.
[37] K. Zhao, M. Pharr, J.J. Vlassak, Z. Suo, Fracture of electrodes in lithium-ion batteries caused by fast charging, J. Appl. Phys. 108 (2010) 073517.
[38] K. Zhao, M. Pharr, S. Cai, J.J. Vlassak, et al., Large plastic deformation in high-capacity lithium-ion batteries caused by charge and discharge, J. Am. Ceram. Soc. 94 (2011) s226.
[39] M.M. Attard, Finite strain–isotropic hyperelasticity, Int. J. Solids Struct. 40 (2003) 4353.
[40] Comsol Multiphysics, Reference Manual, Version 4.4, 2013.
[41] V.A. Sethuraman, M.J. Chon, M. Shimshak, V. Srinivasan, et al., In situ measurements of stress evolution in silicon thin films during electrochemical lithiation and delithiation, J. Power Sources 195 (2010) 5062.
[42] N. Ding, J. Xu, Y. Yao, G. Wegner, et al., Determination of the diffusion coefficient of lithium ions in nano-Si, Solid State Ion. 180 (2009) 222.
[43] C.K. Chan, H. Peng, G. Liu, K. McIlwrath, et al., High-performance lithium battery anodes using silicon nanowires, Nat. Nanotechnol. 3 (2008) 31.
[44] T. Song, J. Xia, J.-H. Lee, D.H. Lee, et al., Arrays of sealed silicon nanotubes as anodes for lithium ion batteries, Nano Lett. 10 (2010) 1710.
[45] C. Yu, X. Li, T. Ma, J. Rong, et al., Silicon thin films as anodes for high-performance lithium-ion batteries with effective stress relaxation, Adv. Energy Mater. 2 (2012) 68.
[46] Y. Yao, M.T. McDowell, I. Ryu, H. Wu, et al., Interconnected silicon hollow nanospheres for lithium-ion battery anodes with long cycle life, Nano Lett. 11 (2011) 2949.
[47] X.H. Liu, H. Zheng, L. Zhong, S. Huang, et al., Anisotropic swelling and fracture of silicon nanowires during lithiation, Nano Lett. 11 (2011) 3312.
[48] S.W. Lee, M.T. McDowell, J.W. Choi, Y. Cui, Anomalous shape changes of silicon nanopillars by electrochemical lithiation, Nano Lett. 11 (2011) 3034.